Near-Threshold Sputter Yields of Ruthenium under Argon and Nitrogen Ion Bombardment

Parikshit Phadke, Jacobus M. Sturm, Robbert W.E. van de Kruijs, Fred Bijkerk

Industrial Focus Group XUV Optics, MESA+ Institute for Nanotechnology, University of Twente, Drienerlolaan 5, 7522NB, Enschede, The Netherlands

Abstract

Ion surface interactions near sputter-threshold are of interest for various plasma facing materials. We report experimental determination of sputter yields for ruthenium films grown on a quartz crystal microbalance and exposed to Ar^+ and N_2^+ ions in the energy range of 50-300 eV. Comparison to semi-empirical models shows agreement to previously reported yields for argon bombardment. In the case of nitrogen, the Yamamura model was modified to account for molecular effects and the yields are found to be between extremes of rigid and non-rigid molecular approximations proposed by Yao. Ex-situ XPS measurements revealed implantation of nitrogen in the ruthenium film after exposure to nitrogen ions . The discrepancy between the models and experimental results for N_2^+ bombardment is explained by an increase in the surface binding energy of the target leading to a chemically reduced sputter yield.

Keywords:
Sputter threshold, Sputter Yields, Quartz microbalance, Ruthenium, Nitrogen

1. Introduction

Terrestrial plasmas occur in a wide range of densities and temperatures. High temperature, dense plasmas in fusion reactors [1], diffuse plasmas induced by extreme ultraviolet radiation [2] and dense low pressure plasmas in

Email address: p.phadke@utwente.nl (Parikshit Phadke)

laboratory ion sources and for electric propulsion [3]. Plasma facing materials (PFMs), such as divertors in fusion reactors are bombarded by hydrogen and deuterium ion species [4], ion lensing systems for electric propulsion technology deteriorate under xenon ion impingement and optics in next generation lithography applications face diffuse hydrogen and nitrogen plasmas [5, 6]. There is, thus, a need to quantify the damage incurred by various PFMs. Sputter yields provide a reasonable estimate of optic material damage due to mass loss when facing diffuse low energy plasmas. However, for reactive ions, chemical effects become dominant near the sputter threshold and need to be accounted for.

While experimental data on sputter yields exist for transition metals under nitrogen ion impingement [7, 8, 9, 10], ruthenium is not well studied. Semi-empirical models account for sputtering by assuming a uniform potential barrier at the surface called the surface binding energy (SBE). This is approximated to the enthalpy of sublimation for most targets. Chemical effects such as compound formation during the sputter process would lead to changes in the SBE. Ruthenium nitride (RuN_x) is predicted to have a positive enthalpy of formation [11]. The formation energy barrier is overcome by the incidence of energetic nitrogen ions or radicals either by magnetron sputtering [12, 13] plasmas or pulsed lasers [14]. The formation of RuN_x during sputter measurements would modify the SBE for such combinations involving reactive species leading to larger deviations in model predictions.

This paper serves as beginning to a series of experiments to study the interaction of nitrogen and other reactive ion species to a variety of PFMs. In this report, we consider the sputtering of ruthenium under argon and nitrogen bombardment and ascertain the validity of semi-empirical models and their approximation of the SBE for compound formation.

2. Experimental Details

The setup of the exposure facility has been described in detail in a previous publication [15]. A commercial 15 cm DC Kaufman-type ion source with a molybdenum three-grid lensing system was used for generating monoenergetic ion beams of argon and nitrogen with energies down to 50 eV at current densities of 100 $\mu A/cm^2$. A residual gas analyser (RGA) was used to measure the background gases in the system, which were dominated by water vapor at a level of 10^{-9} mbar. A faraday cup that also functions as a retarding field energy analyser (FC/RFEA) with an entrance aperture of

1.5 mm diameter was retrofitted onto the source. A 300 nm ruthenium film was deposited on an AT-cut quartz crystal microbalance (QCM) by magnetron sputtering prior to installing it on the source-FC+RFEA assembly. The roughness of the film was not determined. It was shown previously [15] that the sputter yields obtained for a film on a quartz crystal microbalance were similar to the ones determined by exposure of an atomically smooth film on a witness sample. The QCM was placed at the same radial distance from the centre of the source axis as the FC+RFEA. This allowed for the measurement of the current variations throughout the exposure of the ruthenium film to the ions.

The source was operated at a discharge voltage (V_d) of 50 V and 75 V for argon and nitrogen, respectively. The beam was calibrated using the FC+RFEA and the ion energy distributions after a Gaussian fit were found to be mono-energetic with an energy spread between 5-9 eV over the energy range of interest. Analyses of beam contents from similar Kaufman ion sources provide expectation values for argon and nitrogen: At a V_d of 60 V, the concentration of doubly charged ions in the argon plasma is less than 1% [16]. For nitrogen, experiments have shown [17] that while a wide range of parameters influences the composition of the beam, major fractions in current result due to N^+ and N_2^+. Based on their analysis we expect N_2^+ ions making up 80-90% of the beam current for our working conditions with the remainder being N^+. Performing a weighted average on the yields predicted by the Yamamura model (equation 1), for the various species present in the beam, we estimate the deviation of the yield to an upper limit of 18% for nitrogen and 9% for argon at 50 eV due to presence of atomic ions and doubly charged ions respectively. We also estimate a reduction of current density measured at the FC due to resonant neutralization processes [18] up to 2 and 5 percent for argon and nitrogen respectively at a working distance of 7 cm.

Data acquisition of the currents and energy measurements were carried out via a Keithley 2100 micro-ammeter controlled by a MATLAB script running on a personal computer. The QCM frequency response and the ion source were controlled through a LABVIEW program.

The frequency response from the QCM was converted to a thickness value using the Z-match method [15, 19]. Data between the distortions induced by thermal shock at the start and end of the ion irradiation was used to calculate rate of thickness loss (Figure 1) and subsequently, the sputter yields.

The current fluctuations over the dose were estimated to be under 5% for the energies of interest. The exposure energies were selected at random to

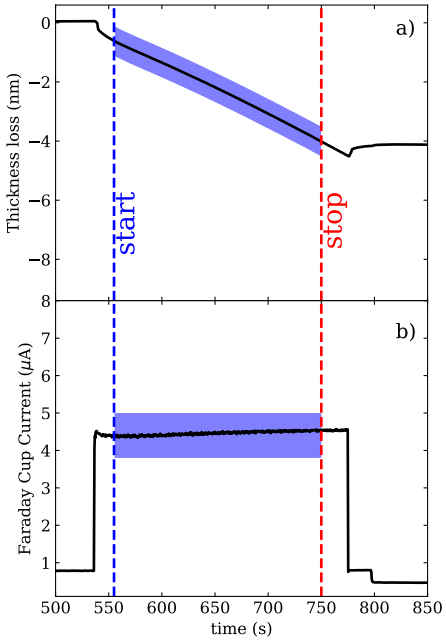

Figure 1: Measurement of thickness loss (a) and ion current (b) made simultaneously with a quartz crystal microbalance and a Faraday cup. The start and stop lines (representative purposes) denote the data used for determining the sputter yield.

avoid systematic errors. In both experiments, the surface oxide was sputter cleaned with 300 eV Ar^+. Additionally, for nitrogen exposures, the surface was treated with 300 eV Ar^+ after each exposure to obtain a clean ruthenium surface prior to each nitrogen ion exposure. Each experiment was carried out until a dose of $1x10^{18}$ ions/cm^2 was irradiated on the surface to ensure sputter yield is measured at steady state and enough statistics are available for the low energy exposures.

At the end of the experiment, the ruthenium coated QCM sample was transferred to an X-Ray Photoelectron Spectroscopy (XPS) setup for characterization. The sample remained in atmosphere for two days before it could be characterized. XPS measurements were done for the ruthenium film at the last energy of irradiation: 60 eV nitrogen ions, using a Thermo-Fisher Theta probe instrument with a beam spot size of 400 μm diameter at an angular range of $\pm 30^\circ$ around an average take-off angle of 53° with respect to the surface normal.

3. Theoretical Models

We choose the Yamamura [20] model for comparison with experimental data because of its extensive usage, and Ecksteins [21] formula for its implementation simplicity. Both build upon Sigmunds original sputter formula to take into account the presence of a sputter threshold. Ecksteins model provided modifications over the Yamamura model by correcting the steep rise of yields above the threshold energy otherwise predicted by the Yamamura model. This was shown to agree well for inert gas ions and self sputtering [22]. It is applied for a wide range of ion-target combinations [23, 24]. The Yamamura model is described as:

$$Y(E) = 0.042 \frac{Q(Z_2)\alpha^*\left(\frac{M_1}{M_2}\right)}{U_s} \frac{S_n(E)}{1 + \Gamma k_e \epsilon^{0.3}} \left(1 - \sqrt{\frac{E_{th}}{E}}\right)^s \tag{1}$$

where M_1 is the mass of the ion, M_2 is the mass of the target atom; E_{th}, s and Q are fitting parameters. E_{th} is the threshold energy for sputtering. S_n is the nuclear stopping power of the target element and the parameter Γ factors in the contribution of reflected ions to the recoil cascade and U_s is the SBE which is usually approximated to the sublimation energy of the target material. And Ecksteins formula takes the form:

$$Y(E) = q s_n^{KrC}(\epsilon_L) \frac{\left(\frac{E}{E_{th}} - 1\right)^\mu}{\frac{\lambda}{w(\epsilon_L)} + \left(\frac{E}{E_{th}} - 1\right)^\mu} \tag{2}$$

where q, E_{th}, μ and λ are used as fitting parameters. s_n^{KrC} is the reduced nuclear stopping power based on the Kr-C interaction potential which is a function of the reduced ion energy, ϵ_L. ϵ_L scales the ion energy with the Lindhard screening length and the masses of the interacting species. Refer to [22] for details. In both cases, Y is the theoretical sputter yield and E is the energy of the incident ion.

While these formulae give a reasonable estimate to the sputter yields for noble gas ions, their accuracy for nitrogen is unreliable due to poor comparison to experimental data. The models have, thus far not been compared with the present ion-target combination. For reactive species, their predictions can be considered a static case, i.e., the yield observed when the first ion hits the target. This would lead to an over-estimation when compound formation occurs, and an under-estimation for chemical sputtering processes.

The SBE would deviate dynamically as the surface composition and ion fluence changes. Compound formation or accumulation of ions would affect the sputter yield [9, 10]. The models are limited in their ability to account for changes in composition of target materials due to implantation or compound formation. The yamamura model provides a surface binding energy term to include a surface potential for sputtering. In order to assess chemical changes by the ion species, a fit to the Yamamura model was performed where the SBE (U_s) was added as a fit parameter.

4. Results and Discussion

Figure 2a shows the sputter yields obtained for ruthenium under argon bombardment. The yields obtained for argon are consistent with data reported by Laegreid [25] for polycrystalline rods and by Wu [15] for e-beam deposited ruthenium. The deviations in the data can be accounted by the changes in film density and roughness in the targets studied [26, 27]. A Markov Chain Monte Carlo (MCMC) code [28] was used to calculate the posterior probabilities of the fitting parameters and only the present dataset was used for ease of comparison with the nitrogen data and prevent any bias by the additional datasets. The fit result is plotted in Figure 2a. The obtained best-fit value for U_s is 7.5±2.8 eV which is similar to the sublimation energy of 6.7 eV used for the initial Yamamura prediction. A sputter threshold of 38.4±1.4 eV obtained from the fit is found to be larger than previous work by ∼15%.

Sputter yields from nitrogen bombardment of ruthenium compared to the Yamamura model are shown in Figure 2b. The expected sputtering by molecular species depends on an effective mass, m*, that lies between two extremes [29] $M_1 \leq m^* \leq 2M_1$ for when the molecule acts as a rigid ensemble with twice the mass of a single atom ($2M_1$) or as two individual atoms (M_1) with half of the original energy. The experimental yields in an ideal situation of no chemical interaction, would lie between these two limiting cases. This molecular effect is dominant for when the vibrational frequency of the molecule is comparable to the interaction time of the collision. From Yao's assumptions [29] of ion-surface interaction times, the molecular effect would occur below 250eV for nitrogen ions. For high energies, atomic and molecular species would sputter equally efficiently. For the comparison with experimental data of nitrogen, parameters in equation 1 were modified to account for the two mass limits and depicted in Figure 2b. Using the same

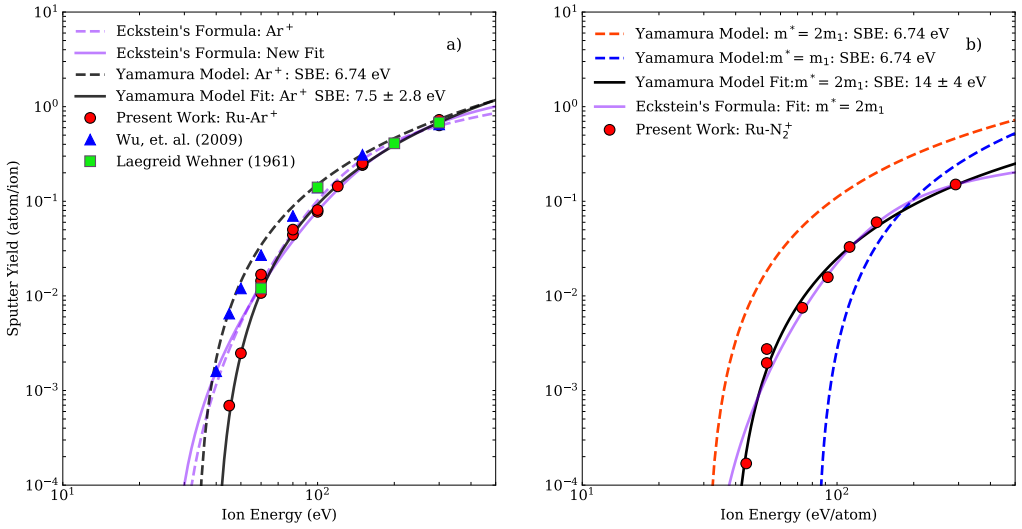

Figure 2: a) Sputter yields obtained from QCM response (circles) compared to reports from Wu (triangles) and Laegreid (squares). The Yamamura (solid black) and Eckstein (solid purple) models with best-fit parameters from Table I are plotted. (b) For N2+ yields, the Yamamura model for a rigid (m* = 2m) and a non-rigid ($m^* = m$) molecule are plotted and compared to a new fit with a modified surface binding energy; New paramters obtained for Eckstein's formula (purple) are also plotted which show marked deviations near the sputter threshold.

procedure for fitting the data as for argon, and using the model with m* = $2M_1$, U_s is found to be 14±4 eV. Q and s remain the same within error for both ion species. A sputter threshold of 37±2 eV was determined from the fit. Eckstein provides a compendium of tabulated values in [24] for the fitting parameters for a wide range of ion and target combinations. However, to our knowledge, no reported best-fit parameter values for a ruthenium and nitrogen combination are available. We provide an estimate to the model parameters using the MCMC approach. The results are summarised in Table I.

Chemical interaction between the ruthenium and nitrogen is evident from the post exposure XPS. The ruthenium 3d spectrum of the QCM exposed to 60 eV nitrogen was compared to a clean ruthenium reference after a Shirley background subtraction. The contribution to the broadening of the metal peaks by oxide formation from an exposure to atmosphere and the nitride formed by the ion exposure experiment are difficult to quantify. The lack of a significant peak shift of the Ru3d peaks indicates that the sample remains

Ion		Yamamura Model				Eckstein Model			
		Q	s	U_s (eV)	E_{th} (eV)	λ	q	μ	E_{th} (eV)
Ar^+		1.31[a]	2.5[a]	6.74[a]	33[a]	0.19[b]	6.84[b]	2.20[b]	27.47[b]
	MCMC	1.86	2.73	7.5	38.4	0.28	8.4	1.88	26.2
	error	±0.68	±0.18	±2.8	±1.4	±0.14	±1.14	±0.35	±5.6
N_2^+		1.31[c]	2.5[c]	6.74[c]	28[c]	-	-	-	-
	MCMC	1.14	2.75	14	37.2	0.31	1.01	2.13	30.0
	error	±0.42	±0.17	±4	±2.2	±0.13	±0.03	±0.17	±4.8

[a]Reference: [15]
[b]Reference: [24]
[c]Reference: [20]

Table 1: Fit parameters with errors obtained from Markov Chain Monte Carlo code after 35,000 steps including a burn-in period of 5000. See [28] for details of the algorithm.

mostly metallic, consistent with transition metal nitrides [13]. The O1s peak for air exposed nitrides shares similar difficulties as the contributions from the oxy-nitride and O-H groups from adsorbed water and hydroxides are challenging to deconvolve. The peaks before and after exposure are shown in Figure 3c for qualitative comparison. The oxygen before exposure contained a metallic oxide at around 529eV which is a dominating contribution after exposure to nitrogen and subsequently atmosphere. The quantification of the nitride and oxynitride is therefore limited to the N1s spectra. Two components of the N1s have been identified, one at 397.3eV corresponding to the nitride and 398.8 eV which is characteristic for an oxynitride for transition metal nitrides exposed to atomsphere [13, 30]. The area under the N1s peak corresponded to 18 atomic percent of nitrogen in the measured sample volume, implying implantation of nitrogen within the target. This is consistent with reports that RuN_x, even though thermodynamically unfavourable, is formed by reactive magnetron sputtering [12].

5. Conclusions

We report sputter yields for ruthenium under argon and nitrogen ion bombardment. Argon shows agreement to the Yamamura model with dis-

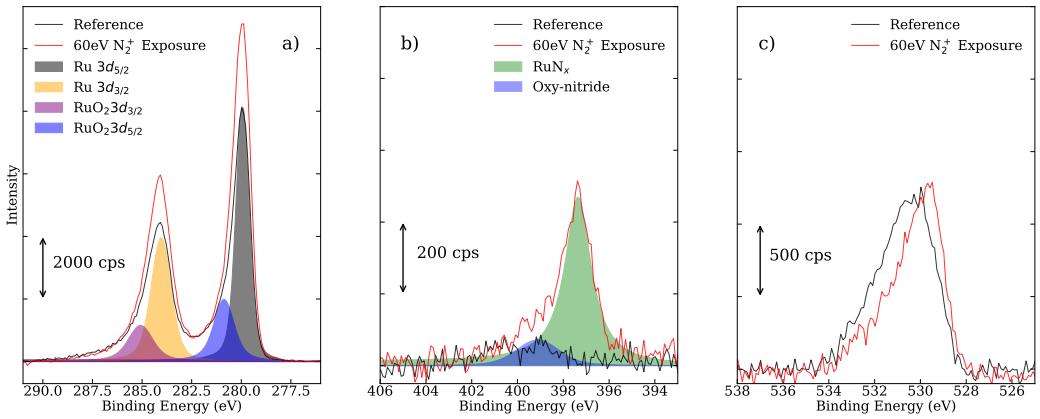

Figure 3: XPS Spectra of Ru coated QCM both measured after exposure to air: with reference (bottom) and 60 eV N_2^+ exposed (top) samples. The Ru3d peaks (a) remain mostly metallic while an N1s (b) peak appears post exposure. See text for details.

crepancies compared to literature that possibly originate from density and roughness variations in the targets analysed. Theoretical yields for nitrogen ions on Ru provide boundaries for expectation values, but over-estimate experimental yields for a rigid molecule approximation. SBE is approximated by sublimation energies for modelling purposes. Transition metals and their nitrides show variation in the sublimation energy as can be seen in case of Zr [31] where the experimentally determined sublimation energy of the metal is 2.7 eV lower than that of the nitride. The approximation of the surface binding energy to the sublimation energy would then be inappropriate for a reactive ion bombaring a metal. Using the SBE (U_s) as a fit parameter showed a change of U_s for ruthenium from argon exposure to nitrogen exposure by 1.8x. We hypothesize that the chemical interaction between nitrogen and ruthenium, as observed by XPS, leads to formation of ruthenium nitride and a change in the SBE.

Investigation of fluence dependence of yields with an estimation of extent of nitridation of ruthenium under nitrogen bombardment is planned for an upcoming series of experiments.

6. Acknowledgement

We acknowledge the support of the Industrial Focus Group XUV Optics at the MESA+ Institute for Nanotechnology at the University of Twente, notably the industrial partners ASML, Carl Zeiss SMT, Malvern PANalytical,

TNO, as well as the Province of Overijssel and the Netherlands Organisation for Scientific Research (NWO). The authors would like to thank Mr. Theo van Oijen for sample preparation and technical support.

[1] C. Watts, V. Udintsev, P. Andrew, G. Vayakis, M. Van Zeeland, D. Brower, R. Feder, E. Mukhin, S. Tolstyakov, Electron density measurements in the ITER fusion plasma, Nuclear Instruments and Methods in Physics Research, Section A: Accelerators, Spectrometers, Detectors and Associated Equipment 720 (2013) 7–10. doi:10.1016/j.nima.2012.12.048.
URL http://dx.doi.org/10.1016/j.nima.2012.12.048

[2] T. H. M. van de Ven, P. Reefman, C. A. de Meijere, R. M. van der Horst, M. V. Kampen, V. Y. Banine, Ion energy distributions in highly transient EUV induced plasma in hydrogen, Journal of Applied Physics 123 (2018) 063301.

[3] D. A. Herman, A. D. Gallimore, Comparison of Discharge Plasma Parameters in a 30-cm NSTAR Type Ion Engine with and without Beam Extraction, 39th AIAA/ASME/SAE/ASEE Joint Propulsion Conference & Exhibit (July) (2003) AIAA 2003–5162.

[4] J. Roth, E. Tsitrone, A. Loarte, T. Loarer, G. Counsell, R. Neu, V. Philipps, S. Brezinsek, M. Lehnen, P. Coad, C. Grisolia, K. Schmid, K. Krieger, A. Kallenbach, B. Lipschultz, R. Doerner, R. Causey, V. Alimov, W. Shu, O. Ogorodnikova, A. Kirschner, G. Federici, A. Kukushkin, Recent analysis of key plasma wall interactions issues for ITER, Journal of Nuclear Materials 390-391 (1) (2009) 1–9. doi:10.1016/j.jnucmat.2009.01.037.
URL http://dx.doi.org/10.1016/j.jnucmat.2009.01.037

[5] M. H. L. Van Der Velden, W. J. M. Brok, J. J. A. M. Van Der Mullen, W. J. Goedheer, V. Banine, Particle-in-cell Monte Carlo simulations of an extreme ultraviolet radiation driven plasma, Physical Review E - Statistical, Nonlinear, and Soft Matter Physics 73 (3) (2006) 1–6. doi:10.1103/PhysRevE.73.036406.

[6] R. C. Wieggers, W. J. Goedheer, M. R. Akdim, F. Bijkerk, P. A. Zegeling, A particle-in-cell plus Monte Carlo study of plasma-induced

damage of normal incidence collector optics used in extreme ultraviolet lithography, Journal of Applied Physics 103 (1) (2008) 013308. doi:10.1063/1.2829783.

[7] K. Dobes, P. Naderer, N. Lachaud, C. Eisenmenger-Sittner, F. Aumayr, Sputtering of tungsten by n+ and n2+ ions: investigations of molecular effects, Physica Scripta 2011 (T145) (2011) 014017.
URL http://stacks.iop.org/1402-4896/2011/i=T145/a=014017

[8] R. Ranjan, J. P. Allain, M. R. Hendricks, D. N. Ruzic, Absolute sputtering yield of ti/ tin by ar+/n+ at 400-700 ev, Journal of Vacuum Science & Technology A 19 (3) (2001) 1004–1007. doi:10.1116/1.1362678.
URL https://doi.org/10.1116/1.1362678

[9] K. Schmid, A. Manhard, C. Linsmeier, A. Wiltner, T. Schwarz-Selinger, W. Jacob, S. Mndl, Interaction of nitrogen plasmas with tungsten, Nuclear Fusion 50 (2) (2010) 025006.
URL http://stacks.iop.org/0029-5515/50/i=2/a=025006

[10] G. Meisl, K. Schmid, O. Encke, T. Hschen, L. Gao, C. Linsmeier, Implantation and erosion of nitrogen in tungsten, New Journal of Physics 16 (9) (2014) 093018.
URL http://stacks.iop.org/1367-2630/16/i=9/a=093018

[11] Y. Zhang, L. Wu, B. Wan, Y. Lin, Q. Hu, Y. Zhao, R. Gao, Z. Li, J. Zhang, H. Gou, Diverse ruthenium nitrides stabilized under pressure: A theoretical prediction, Scientific Reports 6 (2016) 1–9. doi:10.1038/srep33506.
URL http://dx.doi.org/10.1038/srep33506

[12] E. Cattaruzza, G. Battaglin, P. Riello, D. Cristofori, M. Tamisari, On the synthesis of a compound with positive enthalpy of formation: Zinc-blende-like RuN thin films obtained by rf-magnetron sputtering, Applied Surface Science 320 (2014) 863–870. doi:10.1016/j.apsusc.2014.09.158.
URL http://dx.doi.org/10.1016/j.apsusc.2014.09.158

[13] J. H. Quintero, R. Ospina, A. Mello, D. Escobar, E. Restrepo-Parra, Influence of nitrogen partial pressure on the microstructure and morphological properties of sputtered RuN coatings, Surface and Interface Analysis 49 (10) (2017) 978–984. doi:10.1002/sia.6256.

[14] M. G. Moreno-Armenta, J. Diaz, A. Martinez-Ruiz, G. Soto, Synthesis of cubic ruthenium nitride by reactive pulsed laser ablation, Journal of Physics and Chemistry of Solids 68 (10) (2007) 1989–1994. doi:10.1016/j.jpcs.2007.06.002.

[15] S. M. Wu, R. Van De Kruijs, E. Zoethout, F. Bijkerk, Sputtering yields of Ru, Mo, and Si under low energy Ar+ bombardment, Journal of Applied Physics 106 (5) (2009) 0–6. doi:10.1063/1.3149777.

[16] M. Zeuner, J. Meichsner, H. Neumann, F. Scholze, F. Bigl, Design of ion energy distributions by a broad beam ion source, Journal of Applied Physics 80 (2) (1996) 611–622. doi:10.1063/1.362869.

[17] D. Van Vechten, G. Hubler, E. Donovan, Characterization of a 3 cm Kaufman ion source with nitrogen feed gas, Vacuum 36 (11-12) (1986) 841–845. doi:10.1016/0042-207X(86)90123-5.

[18] V. V. Zhurin, Industrial Ion Sources, 2011. doi:10.1002/9783527635726. URL `http://doi.wiley.com/10.1002/9783527635726`

[19] A. Wajid, Improving the accuracy of a quartz crystal microbalance with automatic determination of acoustic impedance ratio, Review of Scientific Instruments 62 (8) (1991) 2026–2033. doi:10.1063/1.1142359.

[20] Y. Yamamura, H. Tawara, Energy dependence of ion-induced sputtering yields from monatomic solids at normal incidence, Atomic Data and Nuclear Data Tables 62 (2) (1996) 149 – 253. doi:https://doi.org/10.1006/adnd.1996.0005.

[21] W. Eckstein, Sputtering yields, Vacuum 82 (9) (2008) 930–934. doi:10.1016/j.vacuum.2007.12.004.

[22] W. Eckstein, R. Preuss, New fit formulae for the sputtering yield, Journal of Nuclear Materials 320 (3) (2003) 209 – 213. doi:https://doi.org/10.1016/S0022-3115(03)00192-2.

[23] Z. Somogyvári, G. A. Langer, G. Erdélyi, L. Balázs, Sputtering yields for low-energy Ar +- and Ne +-ion bombardment, Vacuum 86 (12) (2012) 1979–1982. doi:10.1016/j.vacuum.2012.03.055.

[24] W. Eckstein, Sputtering Yields. In: Sputtering by Particle Bombardment: Experiments and Computer Calculations from Threshold to MeV Energies, Springer Berlin Heidelberg, Berlin, Heidelberg, 2007, pp. 33–187. doi:10.1007/978-3-540-44502-9_3.
URL https://doi.org/10.1007/978-3-540-44502-9_3

[25] N. Laegreid, G. K. Wehner, Sputtering yields of metals for ar+ and ne+ ions with energies from 50 to 600 ev, Journal of Applied Physics 32 (3) (1961) 365–369. doi:10.1063/1.1736012.

[26] V. Shulga, The density effects in polycrystal sputtering, Nuclear Instruments and Methods in Physics Research Section B: Beam Interactions with Materials and Atoms 174 (1-2) (2001) 77–90. doi:10.1016/S0168-583X(00)00458-4.

[27] M. A. Makeev, A. L. Barabási, Effect of surface morphology on the sputtering yields. II. Ion sputtering from rippled surfaces, Nuclear Instruments and Methods in Physics Research, Section B: Beam Interactions with Materials and Atoms 222 (3-4) (2004) 335–354. doi:10.1016/j.nimb.2004.02.028.

[28] D. Foreman-Mackey, D. W. Hogg, D. Lang, J. Goodman, emcee: The MCMC Hammer (2012) 1–15arXiv:1202.3665, doi:10.1086/670067.
URL http://arxiv.org/abs/1202.3665

[29] Y. Yao, Z. Hargitai, M. Albert, R. Albridge, a. Barnes, J. Gilligan, B. Pratt Ferguson, G. Lüpke, V. Gordon, N. Tolk, J. Tully, G. Betz, W. Husinsky, New Molecular Collisional Interaction Effect in Low-Energy Sputtering, Physical Review Letters 81 (3) (1998) 550–553. doi:10.1103/PhysRevLett.81.550.

[30] Y. Kamiura, K. Umezawa, Y. Teraoka, A. Yoshigoe, Characterization of polycrystalline tungsten surfaces irradiated with nitrogen ions by x-ray photoelectron spectroscopy, Materials Transactions 57 (9) (2016) 1609–1614. doi:10.2320/matertrans.M2016107.

[31] K. A. Gingerich, Gaseous Metal Nitrides. II. The Dissociation Energy, Heat of Sublimation, and Heat of Formation of Zirconium Mononitride, The Journal of Chemical Physics 49 (1) (1968) 14–18.

doi:10.1063/1.1669799.
URL http://aip.scitation.org/doi/10.1063/1.1669799